Neutron capture cross sections of ^{74}Ge, ^{76}Ge, and ^{75}As at 25 keV

J. Marganiec,* I. Dillmann,† C. Domingo Pardo,‡ and F. Käppeler
Forschungszentrum Karlsruhe, Institut für Kernphysik, D-76344 Eggenstein-Leopoldshafen, Germany

R. Reifarth
Gesellschaft für Schwerionenforschung, D-64291 Darmstadt, Germany and
Johann Wolfgang Goethe-Universität, D-60438 Frankfurt am Main, Germany

R. Gallino
Dipartimento di Fisica Generale, Università di Torino, Via P. Giuria 1, I-10125 Torino, Italy

M. Pignatari
Keele University, Keele, Staffordshire ST5 5BG, United Kingdom and JINA, University of Notre Dame, Notre Dame, Indiana 46556, USA

P. Grabmayr
Physikalisches Institut der Universität Tübingen, Auf der Morgenstelle 14, D-72076 Tübingen, Germany
(Received 7 January 2009; revised manuscript received 21 April 2009; published 25 June 2009)

The neutron capture cross sections of ^{74}Ge, ^{76}Ge, and ^{75}As have been measured at the Karlsruhe Van de Graaff accelerator by means of the activation technique. The neutron source reaction ^{7}Li$(p, n)^{7}$Be was used for simulating a thermal energy distribution for $kT = 25$ keV to determine the astrophysically relevant stellar cross sections directly. Based on an extended series of activations, consistent results could be obtained, corresponding to Maxwellian average cross sections at $kT = 30$ keV of 37.6 ± 3.9 mb for ^{74}Ge, 21.5 ± 1.8 mb for ^{76}Ge, and 362 ± 19 mb for ^{75}As. These results are more accurate than previous data and are, therefore, important for resolving previous discrepancies. By extrapolation Maxwellian averaged cross sections were derived for thermal energies from 5 to 100 keV. The implications of these results for the s-process abundances in massive stars and for the background conditions in double β decay experiments are discussed.

DOI: 10.1103/PhysRevC.79.065802 PACS number(s): 25.40.Lw, 27.50.+e, 28.20.Fc, 97.10.Cv

I. INTRODUCTION

The nucleosynthesis of heavy elements is dominated by neutron capture reactions in the s and r processes. About half of the abundances between Fe and Bi are produced by the s process, where s stands for the fact that neutron captures occur on a time scale slower than the one for β decay. Accordingly, the reaction path of the s process moves along the valley of β stability [1], in contrast to the r process, where the reaction path runs close to the neutron drip line [2]. Depending on the neutron exposure, the s process can be divided into "weak," "main," and "strong" components, which are responsible for the s abundances in the mass regions $60 \leqslant A \leqslant 90$, $90 \leqslant A \leqslant 208$, and $A = 208, 209$, respectively. However, the separation between these components is not sharp, because the main s process contributes to the weak component in particular in the $80 \leqslant A \leqslant 90$ region [3] and produces also about 50% of ^{208}Pb [3,4].

The Ge isotopes and ^{75}As belong to the weak s process, which takes place during core He and shell carbon burning in massive stars [5] with $M \geqslant 8M_{\odot}$ ($M_{\odot}$ stands for the mass of the sun). In both evolutionary phases, neutrons are produced via the ^{22}Ne$(\alpha, n)^{25}$Mg reaction but under different conditions. At the end of the convective core He burning phase, close to He exhaustion, temperatures rise up to $T \approx 0.3$ GK, that is to thermal energies of $kT = 26$ keV. Under these conditions the ^{22}Ne$(\alpha, n)^{25}$Mg reaction is efficiently activated, resulting in a neutron density of $\approx 10^{6}$ cm^{-3}. In the subsequent convective shell C burning phase, temperatures of ≈ 1 GK are reached, resulting in peak neutron densities up to 10^{12} cm^{-3} [6–8].

The evaluation of reliable abundances for the weak s process requires a full set of neutron capture cross sections between Fe and Sr with uncertainties of less than 10%. The measurements on ^{74,76}Ge and ^{75}As in this work contribute to an improved determination of the s abundances of Ge and As and help to reduce the uncertainties due to propagation effects in the abundance distribution [9]. Furthermore, the cross sections are important for studying the effect of the branching in the reaction path at ^{75}Ge, which opens at neutron densities in excess of 10^{10} cm^{-3}. As noted before, the main s-process component in AGB stars still contributes in the mass region of the weak s process. For the Ge isotopes this fraction is about 6% [3].

The question for the nature of the neutrino, i.e., whether it is its own antiparticle and of Majorana type represents one

*Also University of Lodz, Lodz, Poland; present address: Gesellschaft für Schwerionenforschung, D-64291 Darmstadt, Germany; J.Marganiec@gsi.de
†Now at Fakultät für Physik, Technische Universtät München, D-85747 Garching, Germany.
‡Now at Gesellschaft für Schwerionenforschung, D-64291 Darmstadt, Germany.

of the most urgent problems in physics. This question can be answered by an observation of the neutrinoless double β decay ($2\beta 0\nu$). In this rare reaction one assumes that the antineutrino emitted from the first vertex is captured as neutrino at the second vertex; thus only the two electrons can be detected with a sharp sum energy corresponding to the mass difference $Q_{\beta\beta}$ of the initial and final nucleus. The prerequisite that the neutrinos have mass has been verified through the neutrino oscillations in all flavors.

Direct measurements of the neutrino mass via the tritium decay have reached a limit of 2.2 eV [10,11]. Indirect limits through cosmological constraints can possibly be further reduced by $2\beta 0\nu$ decay experiments [12–14]. In this context, the (n,γ) cross section of ^{76}Ge is of prime interest for a quantitative assessment of the crucial background in double β decay studies on ^{76}Ge.

The stellar cross sections of ^{74}Ge and ^{75}As have been measured by means of the activation technique [15] with uncertainties of 13 and 6%, respectively. However, these data show large discrepancies with respect to other values reported in literature [16]. For example, the only other activation measurement on ^{74}Ge reports a four times smaller stellar cross section with an uncertainty of 70% [17]. For ^{75}As, two recent measurements have been performed, one by activation [17] and one by the time-of-flight (TOF) technique [18]. These cross sections are 45 and 20% smaller than the results of Ref. [15], and discrepancies exceed the quoted uncertainties by more than a factor of 5. In case of ^{76}Ge, two previous activation measurements have been reported with large uncertainties of about 30% [17,19].

In view of these problems, a series of activation measurements was carried out for obtaining improved stellar cross sections of ^{74}Ge, ^{76}Ge, and ^{75}As and to resolve the discrepancies among previous data.

II. EXPERIMENTAL METHOD

The present measurements are based on the activation technique, using the ^{7}Li$(p,n)^{7}$Be reaction [20,21]. This technique is unique for its excellent sensitivity, which allows one to obtain reliable results even for isotopes with very small cross sections, as well as for its excellent selectivity, which has the advantage that samples of natural composition can be used. By combination of both features it is possible to study several reactions simultaneously, be it on different isotopes of an element (as in case of ^{74}Ge and ^{76}Ge) or on isotopes of different elements if an appropriate chemical compound can be used as a sample.

A. Neutron source

The measurements have been performed at the Karlsruhe 3.7-MV pulsed Van de Graaff accelerator in an accurately defined neutron field, which represents a good approximation of the spectrum during central He burning in massive stars. Neutrons were produced via the ^{7}Li$(p,n)^{7}$Be reaction using a proton beam with an energy of $E_p = 1912$ keV, that is 31 keV above the reaction threshold. At this energy, all neutrons are emitted in a forward cone with an opening angle of 120° and a maximum neutron energy of 106 keV. Provided that the production targets are sufficiently thick for the protons to be slowed down below the threshold, the angle-integrated spectrum corresponds almost perfectly to a Maxwell-Boltzmann distribution for a thermal energy of $kT = 25$ keV [20,21] as illustrated in Fig. 1. This feature opens the possibility to measure the Maxwellian averaged cross section directly by activation.

B. Samples

The samples were made from the oxides GeO_2 and As_2O_3, which contain 69.41% germanium and 75.74% arsenic, respectively. Arsenic consists of a single isotope, the composition of natural germanium includes 36.72% of ^{74}Ge and 7.83% of ^{76}Ge [22]. The oxide powders were pressed to pellets 6 and 10 mm in diameter, sandwiched between two gold foils for neutron flux determination via the well-known (n,γ) cross section of ^{197}Au. In total, 15 activations have been performed, 3 for ^{74}Ge (labeled Ge1 to Ge3), 5 for ^{76}Ge (Ge4 to Ge8), and 4 in case of ^{75}As. An additional set of three activations (Ge9 to Ge11) was required for the determination of the partial cross section to the 52.9 s isomer in ^{77}Ge.

In these repeated activations the experimental parameters, i.e., diameter and thickness of the samples and the activation times, have been systematically changed to verify the related corrections and to assess the systematic uncertainties reliably. The sample characteristics and irradiation times are summarized in Table I.

TABLE I. Sample characteristics and irradiation times.

Sample	Diameter (mm)	Thickness (mm)	Mass (mg)	Irradiation time
		^{74}Ge$(n,\gamma)^{75}$Ge		
Ge1	10	1.4	472.25	2.2 h
Ge2	10	0.8	271.65	2.6
Ge3	6	0.9	110.83	2.3
		^{76}Ge$(n,\gamma)^{77}$Ge^{g}		
Ge4	10	0.9	294.44	7.0 h
Ge5	10	0.4	119.85	16.6
Ge6	10	0.2	66.10	8.1
Ge7	6	1.0	118.54	7.4
Ge8	6	0.3	34.69	15.2
		^{76}Ge$(n,\gamma)^{77}$Ge^{m}		
Ge9	10	0.65	218.06	240 s
Ge10	10	1.15	385.23	231
Ge11	6	0.70	83.32	242
		^{75}As$(n,\gamma)^{76}$As		
As1	10	0.8	228.63	2.5 h
As2	10	0.6	187.35	3.9
As3	6	0.9	96.04	14.5
As4	6	0.5	50.01	6.1

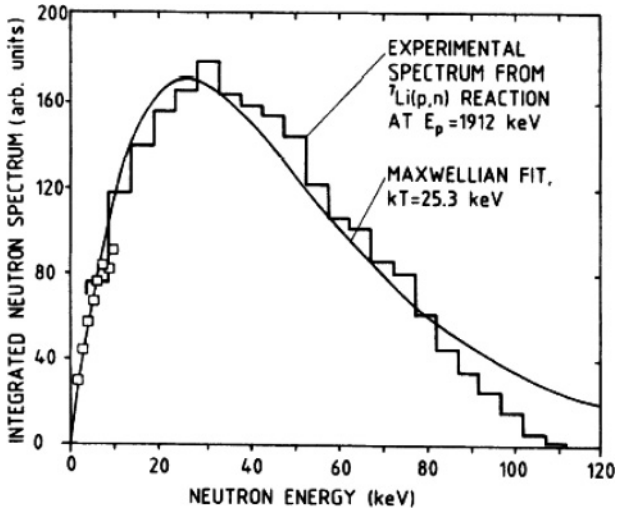

FIG. 1. Neutron spectrum from the ^{7}Li$(p, n)^7$Be reaction at $E_p =$ 1912 keV integrated over the emission cone of 120 opening angle. The spectrum corresponds closely to a Maxwell-Boltzmann distribution for a thermal energy of $kT = 25$ keV.

C. Activations

The measurements were performed in two steps, by irradiation in the well-defined neutron spectrum and by counting of the induced activities. In the present case, the induced activities were determined via the γ rays emitted in the decay of ^{75}Ge, ^{77}Ge^{g}, ^{77} Ge^{m}, and ^{76}As.

1. Irradiation

In the present activation measurements, "thick" LiF targets 10 μm in thickness and 6 mm in diameter were evaporated onto 1.5-mm-thick copper backings. The copper was cooled by lateral heat conduction to a circular water channel outside of the neutron cone, thus avoiding moderation effects of the neutron beam. A sketch of the experimental setup is shown in Fig. 2.

The maximum neutron energy of $E_p = 1912$ keV was adjusted by means of a time-of-flight measurement using a pulsed proton beam 15 ns in width and with a repetition rate of 1 MHz according to the definition given in Refs. [20,21]. Throughout the various activations this setting was permanently controlled via the magnetic field of the analyzing magnet at the exit of the accelerator.

During the irradiation the accelerator was operated in DC mode with beam currents between 80 and 100 μA, yielding a neutron source strength of 2–3 $\times$ 10^9 s^{-1}. Irradiation times of about 2 h, from 7 to 16 h, and from 2.5 to 15.5 h were chosen according to the half-lives of ^{75}Ge ($t_{1/2} = 82.78$ min [23]), ^{77}Ge ($t_{1/2} = 11.30$ h [24]), and ^{76}As ($t_{1/2} = 25.87$ h [25]), respectively. For the additional measurement of the partial cross section to the 52.9 s isomer in ^{77}Ge [24] the irradiation times have been reduced correspondingly.

The samples were irradiated in direct contact with the neutron target at the point of highest flux. In all cases, the geometry was chosen such that the samples were entirely covered by the conical neutron field as indicated in Fig. 2.

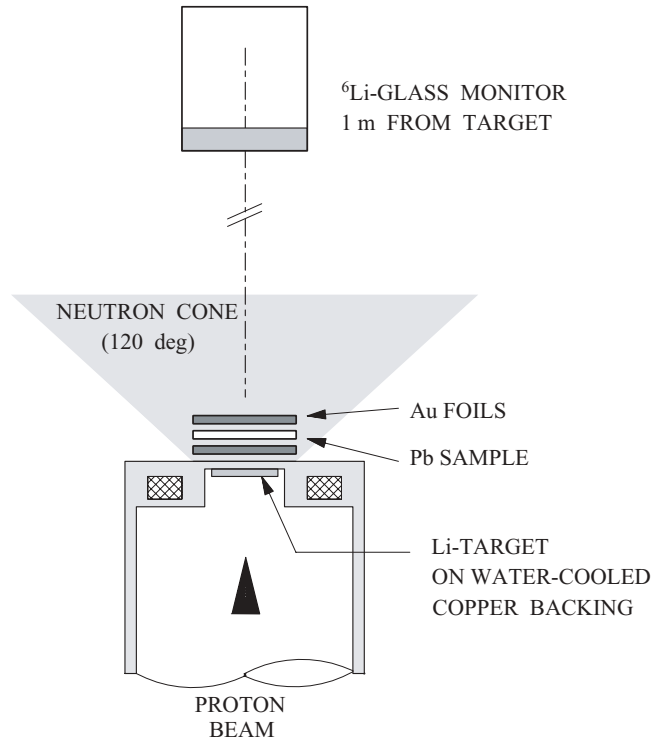

FIG. 2. Experimental setup during the irradiations at the Van de Graaff accelerator.

During the activations, the neutron yield was recorded in time steps of 60 s by means of a ^{6}Li glass detector located 1 m downstream of the target. For the shorter irradiations in runs Ge9–Ge11 the time steps were reduced to 10 s. This information is required to evaluate the correction factor f_b that accounts for the decay of the induced activity during the activation. While this correction can be easily evaluated in a constant neutron field, the time history at an accelerator is influenced by fluctuations in beam intensity and by degradation of the target.

2. Activity measurement

After irradiation, the activity induced in the Ge and As samples as well as in the gold foils was measured in far geometry by means of a shielded high purity Ge detector (HPGe) with 1.7 keV resolution at 1.33 MeV γ-ray energy and a relative efficiency of 30%. The sample-detector distance of 76 mm was exactly defined by a special adapter for the reproducible positioning of the samples. In the relevant energy range between 200 and 600 keV the photo peak efficiencies were determined to $\pm$1.5% using a set of calibrated sources as shown in Fig. 3.

In all cases, γ-ray backgrounds had practically no effect on the uncertainty of the final cross-section values. Summing effects are small for the setup with the single HPGe detector, because of the small solid angle of 0.2 sterad between sample and detector. The corresponding corrections, S_γ, have been determined in simulations with the Monte Carlo code GEANT [26] for all transitions listed in Tables II and V. In each case, 10^8 cascades were followed according to the respective decay

TABLE II. Decay properties of the nuclei produced in the activations.

Product nucleus	$t_{1/2}$	E_γ (keV)	I_γ (%)	Reference
^{75}Ge	82.78 ± 0.04 min	198.6	1.19 ± 0.12	[23]
		264.6	11.4 ± 1.1	
^{75}Ge^{m}	47.7 ± 0.5 s	139.7	99.97 (IT)	[23]
^{77}Ge	11.30 ± 0.01 h	211.03	30.8 ± 1.0	[24]
		215.50	28.6 ± 0.9	
		264.44	53.9 ± 0.5	
^{77}Ge^{m}	52.9 ± 0.6 s	159.7	19 ± 2 (IT)	[24]
		215.5	21.6 ± 3.3 (β^-)	
^{76}As	25.87 ± 0.04 h	559.1	45 ± 2	[25,46]
^{197}Au	2.69517 ± 0.00021 d	411.8	95.58 ± 0.12	[47]

schemes and the efficiency for detecting a particular transition was compared to the efficiency obtained by simulating 10^8 single transitions. The resulting corrections shown in Table III are affecting the capture cross sections by 2 to 3%. The related uncertainties were neglected.

The weak activities from the decay of the isomeric state in ^{77}Ge that were obtained in the short irradiations Ge9 to Ge11 have been counted with higher efficiency using a system of two HPGe clover detectors, which were mounted face to face in close geometry. The samples were positioned in the center of the system by an accurately designed holder. The system was calibrated in the same way as the single detector, but the close geometry implied a somewhat larger uncertainty for the efficiency of 2%. This value was conservatively adopted in data analysis for the γ counting in general.

In case of the Ge clover setup summing effects can, in principle, be very crucial due to the close geometry and the high γ-ray efficiency (Fig. 3). Luckily, almost no cascade transitions are involved in the decay of the isomeric state in ^{77}Ge. The transitions used for analysis were the 159.7-keV line from internal decay and the 215.5-keV transition in ^{77}As with a cascade contribution of less than 0.4%.

The cross sections were obtained from the most intense γ-ray lines emitted in the decays of ^{75}Ge, ^{77}Ge, and ^{76}As. The decay properties used in data analysis are summarized in Table II.

The excellent sensitivity of the measurement is illustrated in Figs. 4 and 5. The statistical uncertainties were always much smaller than the respective systematic uncertainties (see below).

TABLE III. Measured cross sections of ^{74}Ge, ^{76}Ge, and ^{75}As and the corresponding total uncertainties.

Reaction	Activation	γ-ray energy (keV)	Corrections		Measured cross section (mb)	Mean value (mb)
			K_γ	S_γ		
^{74}Ge$(n,\gamma)^{75}$Ge	Ge1	198.6	0.955	0.976	39.1 ± 4.1	
		264.6	0.964	0.985	36.8 ± 3.7	
	Ge2	198.6	0.974	0.976	41.5 ± 4.4	
		264.6	0.979	0.985	38.4 ± 3.9	
	Ge3	198.6	0.970	0.976	39.5 ± 4.3	
		264.6	0.977	0.985	37.4 ± 3.9	38.6 ± 4.0
^{76}Ge$(n,\gamma)^{77}$Ge^{g}	Ge4	211.0	0.973	0.977	11.8 ± 0.5	
		215.5	0.974	0.961	11.4 ± 0.5	
		264.4	0.978	0.969	11.9 ± 0.5	
	Ge5	211.0	0.989	0.977	12.0 ± 0.6	
		215.5	0.989	0.961	12.2 ± 0.6	
		264.4	0.991	0.969	11.8 ± 0.5	
	Ge6	264.4	0.995	0.969	11.8 ± 0.5	
	Ge7	264.4	0.975	0.969	12.4 ± 0.5	
	Ge8	211.0	0.993	0.977	11.8 ± 0.6	11.9 ± 0.4[a]
^{76}Ge$(n,\gamma)^{77}$Ge^{m} (β^-)	Ge9	159.7	0.973		11.6 ± 1.5	
		215.5	0.980		12.4 ± 2.0	
	Ge10	159.7	0.953		13.2 ± 1.7	
		215.5	0.966		13.5 ± 2.1	
	Ge11	159.7	0.972		13.0 ± 1.7	
		215.5	0.979		14.3 ± 2.3	12.8 ± 1.8
^{75}As$(n,\gamma)^{76}$As	As1	559.1	0.989	0.971	370 ± 20	
	As2		0.991	0.971	372 ± 20	
	As3		0.987	0.971	371 ± 20	
	As4		0.993	0.971	370 ± 20	371 ± 20

[a]Value includes the contribution from IT decay of isomer (Table II).

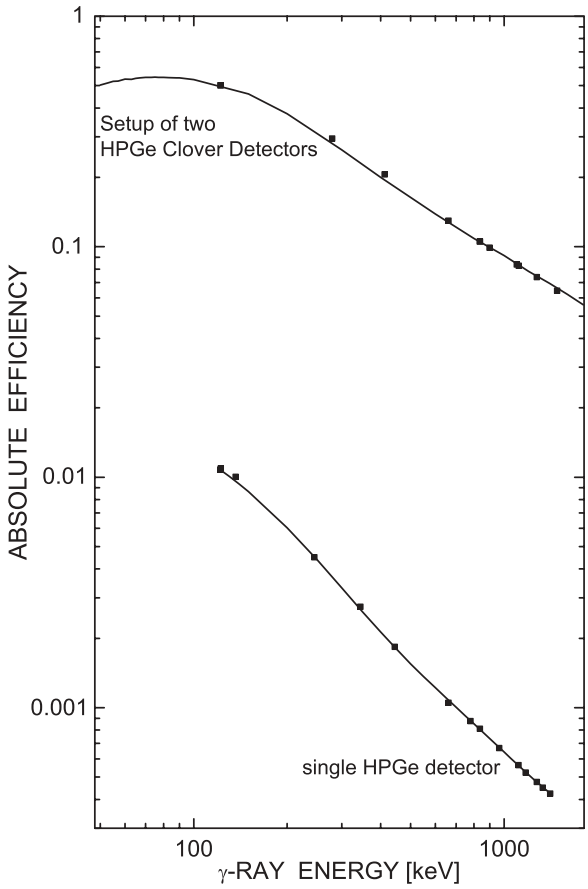

FIG. 3. Photopeak efficiencies for the single HPGe detector and for the sum over the eight individual crystals of the two Clover detectors. The Monte Carlo simulations for the Clover setup were normalized to the data points measured with calibrated sources. The error bars of the measured data points correspond to the size of the symbols.

III. DATA ANALYSIS

The number of activated nuclei at the end of an irradiation can be written as:

$$A = \phi_{\rm tot} N \sigma f_b, \tag{1}$$

where $\phi_{\rm tot} = \int_0^{t_a} \phi(t)dt$ is the time integrated neutron flux, N the sample thickness, and σ the capture cross section averaged over the experimental neutron spectrum. The factor f_b accounts for the decay of activated nuclei during the activation time t_a as well as for variations in the neutron flux,

$$f_b = \frac{\int_0^{t_a} \phi(t) {\rm e}^{-\lambda(t_a - t)} dt}{\int_0^{t_a} \phi(t) dt}. \tag{2}$$

After irradiation the activity is measured in a low background counting station. The number of counts in a given γ-ray line is

$$C = A K_\gamma S_\gamma \varepsilon_\gamma I_\gamma (1 - {\rm e}^{-\lambda t_m}) {\rm e}^{-\lambda t_w}, \tag{3}$$

where ε_γ denotes the detection efficiency, S_γ the summing corrections, I_γ the intensity per decay, t_w the waiting time between irradiation and activity measurement, and λ the decay

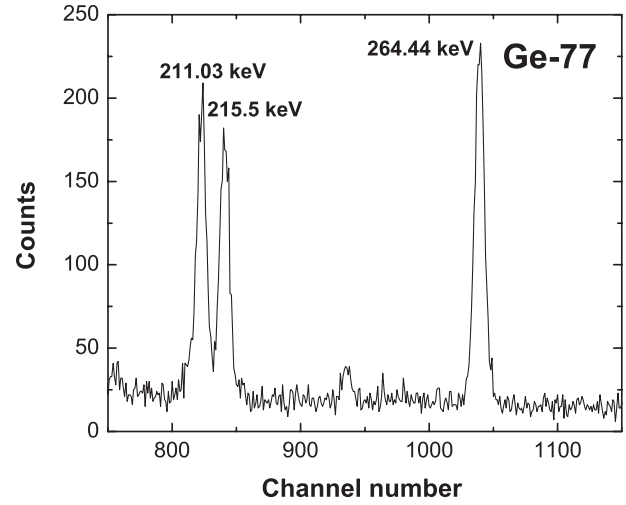

FIG. 4. The γ-ray spectrum of of ^{77}Ge after activation Ge5 showing the lines at 211, 215, and 264 keV.

rate. The γ-ray self absorption of the sample is described by the correction factor

$$K_\gamma = \frac{1 - {\rm e}^{-\mu x}}{\mu x}, \tag{4}$$

which can be applied for disk samples of thickness x in far geometry from the detector. While this was the case for the single HPGe detector, the close geometry of the clover system used for counting the activities from the irradiations Ge9 to Ge11 required a different approach. For this geometry the absorption corrections were obtained by detailed GEANT simulations [26] of the complete setup [27]. The respective γ-ray absorption coefficients μ were taken from Ref. [28].

Because all measurements are performed relative to ^{197}Au as a standard, one obtains

$$\frac{A_i}{A_{\rm Au}} = \frac{\sigma_i}{\sigma_{\rm Au}} \frac{N_i}{N_{\rm Au}} \frac{f_{b_i}}{f_{b_{\rm Au}}}, \tag{5}$$

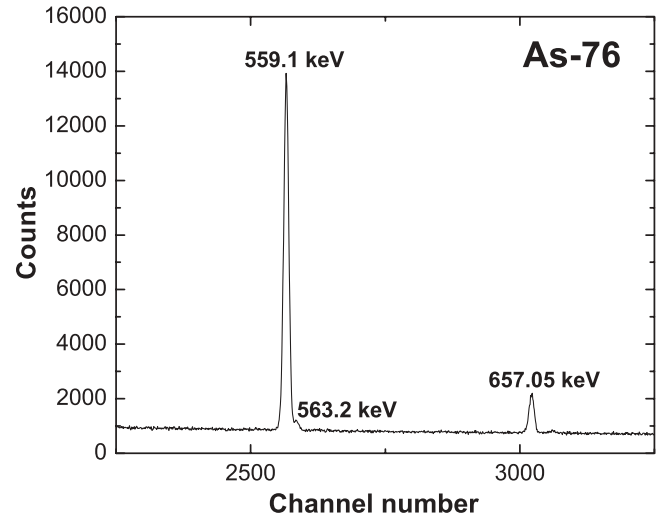

FIG. 5. The γ-ray spectrum of ^{76}As after activation As3 illustrates the very good counting statistics for the lines at 559 and 657 keV. The weak ^{76}As line at 563.2 keV was discriminated by the fit.

TABLE IV. Compilation of uncertainties.

Source of uncertainty	Related uncertainty (%)			
	^{74}Ge	^{76}Ge^{g}	^{76}Ge^{m}	^{75}As
Au standard	2.0	2.0	2.0	2.0
γ efficiency, ε_γ	2.0	2.0	2.0	2.0
γ self-absorption, K_γ	$\leqslant$0.1	$\leqslant$0.1	$\leqslant$0.1	$\leqslant$0.1
γ-ray intensity per decay, I_γ	9.7–10.1	0.9–3.2	10.5–15.2	4.4
Irradiation history, time factor, f_b	0.08–0.09	0.05–0.13	5.0–5.2	0.03–0.19
Half-life $t_{1/2}$	0.05	0.09	1.1	0.34
Counting statistics	1.3–2.0	1.0–3.7	2.0–2.3	0.5–1.0
Total uncertainty	10.5	3.8	14.1	5.5

where A_i and A_{Au} are determined by Eq. (1) via the measured line intensities. The gold cross section averaged over the quasistellar spectrum used in this work is accurately known to be 586 ± 8 mb [21].

The cross section σ_{exp} for isotope i obtained from this relation represents an average over the neutron spectrum used for the irradiation and can be expressed as

$$\sigma_i = \sigma_{\mathrm{exp}} = \frac{\int \sigma(E)\phi(E)dE}{\int \phi(E)dE}, \tag{6}$$

where $\sigma(E)$ is the differential cross section and $\phi(E)$ is the experimental spectrum described in Sec. II A.

IV. RESULTS AND DISCUSSION

A. Measured cross sections

The results obtained in the 15 activations are summarized in Table III together with the corrections for γ-ray self absorption. The fact that the results of the repeated activations with modified experimental conditions (Table I) are consistent within the quoted uncertainties confirms the corrections for finite sample size and self shielding effects. The negligible effect of the different irradiation times shows that uncertainties of the half-lives of the product nuclei do not contribute noticeably to the final cross-section uncertainties.

Because neutron capture on ^{76}Ge populates the ground state and the 52.9 s isomer in ^{77}Ge, both partial cross sections were determined separately. The isomeric ratio, which is defined as the ratio of the partial cross section to the isomer and the total capture cross section,

$$IR(^{76}\mathrm{Ge}) = \frac{\sigma^m}{\sigma^{\mathrm{tot}}} = 0.52 \pm 0.09$$

is slightly smaller than the value at thermal energy (0.65 ± 0.08 [29]) but still consistent within uncertainties.

The various contributions to the uncertainties of the present results are listed in Table IV. For the ^{74}Ge cross section as well as for the partial cross section to the 52.9 s isomer in ^{77}Ge the uncertainties are completely dominated by the uncertainties of the γ-ray intensities I_γ. If these parameters are improved in future, it will be possible to improve the accuracy of the present values correspondingly. The partial cross section of ^{76}Ge to the ground state of ^{77}Ge and the cross section of ^{75}As are much more accurate in this respect, because the related uncertainties are comparable to those of the Au cross section and the γ-ray efficiency. Accordingly, total uncertainties of 3.8 and 5.5% could be reached for these reactions.

It is worth noting that an inconsistency in the γ-ray intensities of the ^{77}Ge^{g} decay was found during data analysis. As illustrated in Table V the cross section values obtained for the weaker lines at 367 and 558 keV are systematically higher than those determined via the strong lines below 300 keV. Corrected intensities are suggested in column four of Table V by normalization to the cross-section average derived from the lines at 211, 215, and 264 keV. The comparison to previous data are presented in the following section along with the discussion of the Maxwellian average cross sections.

B. Maxwellian averaged cross sections at $kT = 30$ keV

Though the experimental spectrum represents a very good approximation of the thermal spectrum for $kT = 25$ keV, the cutoff at 106 keV requires a small correction, especially if the energy dependence of the investigated cross section differs from that of the gold reference cross section. The problem of the cross-section shape is also important for the extrapolation of the measured 25-keV values to $kT = 30$ keV, which is commonly used for the comparison of s-process data, as well as for the further extrapolation covering the full temperature range of the various s-process scenarios.

For the calculation of the final Maxwellian averaged cross sections (MACS)

$$\langle\sigma\rangle_{kT} = \frac{\langle\sigma v\rangle}{v_T} = \frac{2}{\sqrt{\pi}} \frac{\int_0^\infty \sigma(E_n) \times E_n \times \exp(-E_n/kT)dE_n}{\int_0^\infty E_n \times \exp(-E_n/kT)dE_n} \tag{7}$$

TABLE V. Suggested γ decay properties of ^{77}Ge^{g}.

E_γ (keV)	I_γ (%)	Deduced cross section (mb)	Suggested I_γ (%)	
			This work	Ref. [45]
211.03	30.8 ± 1.0	11.9 ± 0.5	–	
215.50	28.6 ± 0.9	11.9 ± 0.5	–	
264.44	53.9 ± 0.5	12.0 ± 0.5	–	
367.4	14.0 ± 0.3	13.0 ± 0.5	15.3 ± 0.4	16.3 ± 2.7
558.02	16.1 ± 0.4	13.9 ± 0.6	18.8 ± 0.5	18.7 ± 3.2

TABLE VI. Normalization factors NF for the evaluated and calculated data sets used to extrapolate the MACS to lower and higher temperatures.

Isotope	JEFF-3.1	JENDL-3.3	ENDF-B/VII.0	NON-SMOKER
^{74}Ge	3.17	3.32	0.83	0.92
^{76}Ge	2.32	2.68	1.29	0.94
^{75}As	0.91	0.80	0.79	1.28

the spectrum correction was obtained by using the differential (n, γ) cross sections of the isotopes under investigation, $\sigma_{n,\gamma}(E_n)$, from evaluated data libraries or from theoretical calculations. These data sets were first normalized to the new experimental values and then used to obtain the corresponding Maxwellian averages.

In a first step, the differential cross sections from the online data libraries JEFF/3.1 (www.nea.fr/html/dbdata/JEFF/), JENDL/3.3 (wwwndc.tokai-sc.jaea.go.jp/jendl/), and ENDF/B-VI.8 (www.nndc.bnl.gov/) were folded with the experimental neutron spectrum, yielding the normalization factors NF $= \sigma_{\rm exp}/\sigma_{\rm eval}$ listed in Table VI. The uncertainties of the corrections for transforming the measured value into the MACS at $kT = 25$ keV were always less than 0.5%, practically negligible compared to the experimental uncertainties.

The final stellar (n, γ) cross sections at $kT = 25$ keV are 41.1 ± 4.6 mb for ^{74}Ge, 23.3 ± 2.0 mbarn for ^{76}Ge, and 404 ± 21 mb for ^{75}As, respectively (Table VII). The corresponding values for $kT = 30$ keV, which are traditionally used for comparison [30], are 37.6 ± 3.9, 21.5 ± 1.8, and 362 ± 19 mb.

The present MACSs are systematically smaller than the previous values of Ref. [16], which are essentially

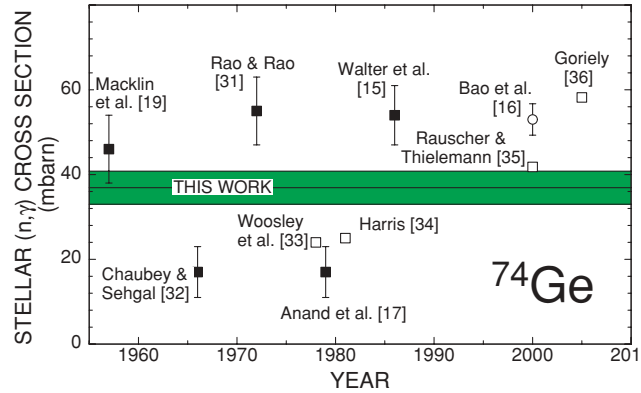

FIG. 6. (Color online) Comparison of the present MACS at $kT = 30$ keV for ^{74}Ge and previous data. Experimental and theoretical values are indicated by black and open squares, respectively. The open circle denotes the recommended MACS from the compilation of Ref. [16]. Note that the values of Refs. [15,17,19,31,32] were renormalized to the presently adopted gold reference cross section [21].

based on measurements performed in the 1970s and 1980s (Refs. [15,17,31], [15,17], and [15,17,18] for ^{74}Ge, ^{76}Ge, and ^{75}As, respectively), whereas data prior to 1970 [19,32] were considered to be more uncertain. For consistency, all data used in the following comparison have been normalized to the presently adopted gold reference cross section [21].

The comparison in Figs. 6, 7, and 8 includes also theoretical cross sections calculated with the Hauser-Feshbach statistical model (HFSM) [33–36]. Typical uncertainties of these results are 25 to 30%.

The experimental ^{74}Ge cross sections for $kT = 30$ keV fall essentially into two groups, around 20 mb [17,32] and

TABLE VII. Maxwellian averaged cross sections obtained by normalization of the NON-SMOKER values to the measured cross section at $kT = 25$ keV.[a]

	Thermal energy (keV)										
	5	10	15	20	25	30	40	50	60	80	100
					^{74}Ge$(n, \gamma)^{75}$Ge						
This work[b]	106 ± 12	70.2 ± 7.3	55.0 ± 5.8	46.9 ± 5.0	41.1 ± 4.6	37.6 ± 3.9	32.6 ± 3.4	29.0 ± 3.1	26.3 ± 2.8	23.4 ± 2.8	22.0 ± 3.0
Ref. [16]	149	99	78	66	58	53 ± 7	46	41	37	33	31
SEF[c]	1.000	1.000	1.000	1.000	1.000	1.000	1.000	1.000	1.000	0.999	0.995
					^{76}Ge$(n, \gamma)^{77}$Ge						
This work[b]	58.0 ± 5.8	39.8 ± 3.4	31.3 ± 2.7	26.7 ± 2.3	23.5 ± 2.0	21.5 ± 1.8	18.2 ± 1.5	16.3 ± 1.4	15.0 ± 1.3	13.0 ± 1.1	12.3 ± 1.1
Ref. [16]	89	61	48	41	36	33 ± 15	28	25	23	20	19
SEF	1.000	1.000	1.000	1.000	1.000	1.000	1.000	1.000	1.000	1.000	0.999
					^{75}As$(n, \gamma)^{76}$As						
This work[d]	1124^{+60}_{-65}	725^{+38}_{-52}	559^{+29}_{-36}	466^{+24}_{-27}	404^{+21}_{-21}	362 ± 19	304^{+17}_{-16}	266^{+16}_{-14}	247^{+13}_{-17}	211^{+11}_{-18}	174^{+14}_{-11}
Ref. [16]	1790	1137	878	732	635	568 ± 35	478	418	389	331	273
SEF	1.000	1.000	1.000	1.000	1.000	0.999	0.997	0.990	0.978	0.941	0.894

[a]Uncertainties of the extrapolated values are estimated from the differences between results obtained with normalized evaluated cross sections from data libraries and with previously recommended MACSs [16].
[b]Values of Ref. [16] normalized to measured value. Uncertainties of extrapolation estimated from differences to theoretical data from Ref. [35].
[c]SEF values from Ref. [16].
[d]Values of Ref. [16] normalized to measured value. Uncertainties of extrapolation estimated from differences to evaluated data libraries JEFF/3.1, JENDL/3.3, and ENDF/B-VI.8.

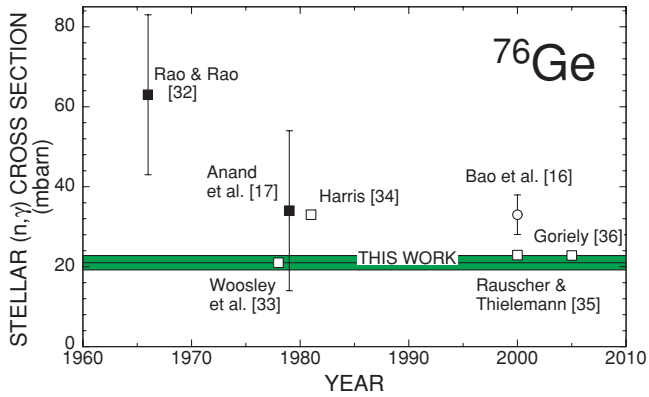

FIG. 7. (Color online) Comparison of the present MACS at $kT = 30$ keV for ^{76}Ge and previous data. Experimental and theoretical values are indicated by black and open squares, respectively. The open circle denotes the recommended MACS from the compilation of Ref. [16]. Note that the values of Refs. [17,19] were renormalized to the presently adopted gold reference cross section [21].

near 50 mb [15,19,31] as shown in Fig. 6. Because a detailed description of these measurements is missing, it is difficult to discuss possible reasons for the discrepancies and for the differences to the present value of 37.6 ± 3.9 mb. This holds even for the better documented work of Walter *et al.* [15], which was performed with the same technique as applied here. If their analysis is updated with the present values for half-life gold cross section, and decay intensity, their result would be reduced by 5%. Because only a single activation was performed in Ref. [15], there is no hint for an explanation of the remaining discrepancy with respect to the consistent average of the repeated activations reported here. In summary, the present MACS of ^{74}Ge is 30% lower than recommended in Ref. [16], but the comparably large uncertainties of the γ-decay intensities are a persisting problem for activation measurements on this isotope.

So far, only two very uncertain measurements of the ^{76}Ge cross section have been reported in literature [17,32]. For the

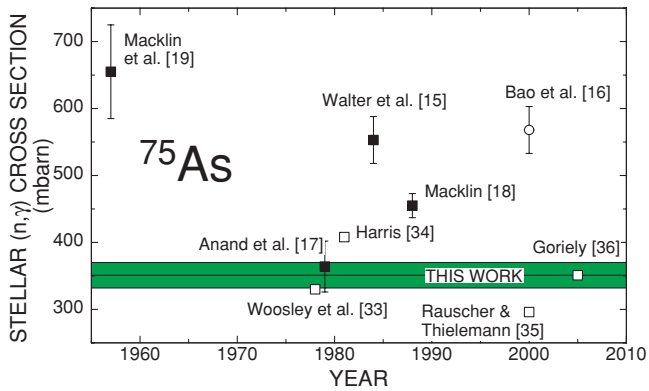

FIG. 8. (Color online) Comparison of the present MACS at $kT = 30$ keV for ^{75}As and previous data. Experimental and theoretical values are indicated by black and open squares, respectively. The open circle denotes the recommended MACS from the compilation of Ref. [16]. Note that the values of Refs. [15,17,19] were renormalized to the presently adopted gold reference cross section [21].

theoretical HFSM approach it was noted that the level density in the case of ^{76}Ge(n,γ) reactions is already so low that these results become doubtful below $kT = 13$ keV, i.e., in the lower range of *s*-process temperatures [35]. As shown in Fig. 7, however, the HFSM calculations are found to agree better with the present result than with the recommended rate in Ref. [16], which was derived from the measurement of Anand *et al.* [17].

From the previous activation measurements on ^{75}As only the result of Ref. [17] agrees with the present cross section, whereas the other two are much too high [15,19]. Similar to the case of ^{76}Ge, the correction of the value given in Ref. [15] with updated information on the decay intensities and the gold reference cross section leads to a slightly smaller cross section than in the original paper, but still far outside the present uncertainties (Fig. 8). The only time-of-flight measurement on ^{75}As [18] yielded a value that lies in between the old activation data and the present result, but also clearly outside the quoted uncertainties. In view of the consistent results from the series of four activations reported here, the new cross section suggests that the existing discrepancies are now resolved in favor of a lower cross section value. This is also supported by the much better agreement with HFSM calculations.

C. Extrapolation of MACS values

While the energy dependence of the cross sections has a comparably small effect for the spectrum corrections at $kT = 25$ keV, it becomes a crucial problem for the extrapolation toward lower and higher thermal energies to cover the full range of *s*-process temperatures from $kT = 5$ to 100 keV. In case of the isotopes investigated here the energy dependencies of the evaluated data sets (JEFF/3.1, JENDL/3.3, and ENDF/B-VI.8) and of the NON-SMOKER calculations are rather similar, but some of the evaluated data deviate by more than a factor of three from the present experimental results as illustrated by the normalization factors NF listed in Table VI.

Because it is not obvious, which trend with kT is to be preferred, and because it is beyond the scope of this article to trace the origin of the differences between various evaluations, the recommended values, which have been used for the *s*-process calculations discussed in the next section, were extrapolated following the Bao *et al.* compilation [16]. This choice was motivated by the fact that the available TOF data were considered in Ref. [16] as well.

For ^{74}Ge and ^{76}Ge, the uncertainties of the extrapolated MACSs were estimated by means of the difference to the theoretical cross sections obtained with the statistical model code NON-SMOKER [35]. For ^{75}As these uncertainties included the comparison with the upper and lower bounds obtained with the evaluated cross sections from the data libraries. The uncertainties of the recommended values are, therefore, composed of the experimental uncertainties originating from the measured data and of the contributions due to the extrapolation procedure.

Corrections due to the thermal population of excited states are of minor importance for the cross sections investigated here. While the stellar enhancement factors (SEF) are negligible for ^{74}Ge and ^{76}Ge, the SEFs for ^{75}As are slowly increasing

above $kT = 40$ keV to reach 10% at the temperature maximum during shell C burning [16].

V. IMPLICATIONS IN ASTROPHYSICS AND DOUBLE β DECAY STUDIES

A. The *s*-process abundance pattern in massive stars

The effect of the new cross sections on the abundance distribution of the weak *s* process was calculated for a stellar model of a $25M_{\odot}$ star using the postprocessing code described in Refs. [6,37,38]. The final situation after the shell C burning phase is compared in Fig. 9 to the results obtained with the previous set of cross sections from Ref. [16].

The new MACS of ^{74}Ge leads to an increase of the *s* abundance of this isotope by about 30%, resulting in a slightly higher contribution (5% at most) of the weak *s* process to solar Ge compared to the value obtained with the previous cross section. However, the new MACS of ^{74}Ge gives rise to a significant propagation wave in the abundance distribution, which leads to a reduction of the *s* abundances by about 15% on average.

In most *s*-process scenarios, the reaction path does not include ^{76}Ge because of the short half-life of ^{75}Ge. Therefore, ^{76}Ge is often considered as an *r*-only isotope. However, in the high neutron density zones of C shell burning in massive stars, the branching at ^{75}Ge is open and ^{76}Ge is efficiently produced by the neutron capture channel. Nevertheless, the *s* abundance of ^{76}Ge does not significantly change compared to previous calculations, because the enhancement due to the smaller MACS of this work is partly compensated by the reduced reaction flow due to the propagation wave from ^{74}Ge. The same argument holds for ^{75}As as well, where the new MACS is also lower than previously adopted.

The range of uncertainties, which are caused by the extrapolation from the measured energy at $kT = 25$ keV to the higher energies around $kT = 90$ keV during shell C burning,

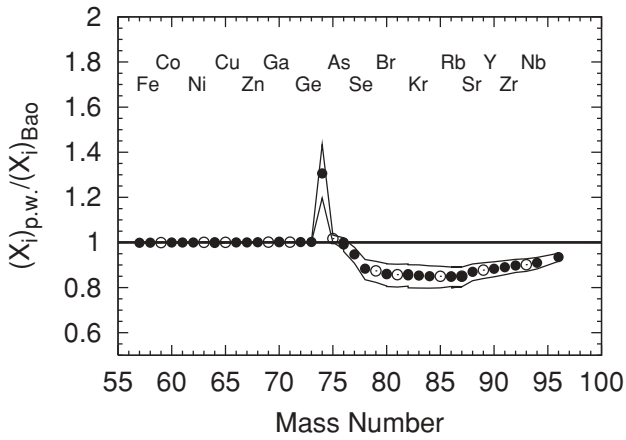

FIG. 9. The present *s*-process distribution at the end of C shell burning ("p.w.") compared to the distribution obtained with the previous MACS of ^{74,76}Ge and ^{75}As [16]. Variations due to the present uncertainties of the MACS at $kT = 30$ and 90 keV are indicated by thin lines. Elements with even and odd Z are distinguished by black and open symbols, respectively.

has been estimated by variation of the MACS within the uncertainties given in Table VII. The combined effect of these uncertainties is indicated by the thin lines in Fig. 9.

Because the new MACSs of ^{74,76}Ge are considerably smaller than the previously recommended values [16] it can be expected that this holds for the cross section of ^{72}Ge as well. If confirmed, this may lead to a significant enhancement of the propagation wave discussed before. In view of these remaining problems, complementary TOF measurements are clearly needed for a more reliable description of the abundance distribution of the weak *s* process in massive stars.

B. Neutrinoless double β decay

A claim [39,40] for the observation of neutrinoless double β decay ($2\beta0\nu$) in ^{76}Ge and the extraction of a half-life of $t_{1/2} = 1.2 \times 10^{25}$ yr with a confidence level of 4.2σ is heavily disputed [41,42]. The GERDA Experiment [43] aims at the verification of this claim, while other experiments focus on the $2\beta0\nu$ decay in different nuclei [12–14]. ^{76}Ge is a favored candidate because of the high energy and position resolution, which has been achieved by previous developments in detector technology. In this calorimetric type of experiments, source and detector are identical.

These rare-decay experiments have to be performed in very clean environments and particular care must be taken against radiation induced by cosmic particles. Even in underground laboratories with large overburden, such as the Laboratori Nazionali di Gran Sasso (LNGS) with 3500 m of water equivalent, there exists a non-negligible flux of cosmogenically produced neutrons. The concept of GERDA is based on the deployment of naked diodes made from material enriched to 86% in ^{76}Ge, which are immersed in liquid argon inside a stainless steel cryostat 4 m in diameter. The cryoliquid serves as coolant and as shield and might later be expanded into an active veto. The cryostat is located inside a water tank 10 m in diameter and about 9 m in height to shield radiation from the decay products in the rock and to serve as active muon veto. In the GERDA Experiment a background index of better than 10^{-3} counts/(keV kg yr) is envisaged, about a factor of 100 better than that of Refs. [39,40]. According to Monte Carlo simulations the use of liquid argon instead of liquid nitrogen as coolant doubles the neutron flux in the detectors with $E \leqslant 1$ keV to about 40 neutrons/(kg yr). This has to be compared to 360 neutrons/(kg yr) in the range from 1 keV to 2 MeV.

One of the crucial background contributions is due to neutron capture on ^{76}Ge, which is producing 2037-keV γ rays, rather close to the expected line at the $Q_{\beta\beta}$ value of 2039 keV. Based on the claim in Refs. [39,40] we expect for the $2\beta0\nu$ decay in ^{76}Ge less than 1 count/(kg yr) in a 5-keV range of interest at $Q_{\beta\beta}$. GEANT simulations using evaluated cross sections from Ref. [44] predict a rate of 0.7 neutron captures/(kg yr).

The background simulations will, therefore, benefit from the improved accuracy of the present cross section results. Because it is plausible that the background level scales with the ^{76}Ge(n, γ) cross section, a lower background is to be expected from the present data. In parallel, a neutron capture experiment at thermal energies will provide a complementary

cross-section value as well as information on the prompt and delayed γ cascades [45]. A preliminary analysis this experiment reports the same inconsistencies in the γ-ray intensities for the 367- and 558-keV lines in the decay of ^{77}Ge as was found in this work (Table V). All data together will be instrumental for the reliable assessment of the GERDA Experiment and will possibly permit a handle for active background suppression.

VI. SUMMARY

The (n, γ) cross sections of ^{74}Ge, ^{76}Ge, and ^{75}As were measured by means of the activation technique, using the quasistellar neutron spectrum with the ^{7}Li$(p, n)^{7}$Be reaction. Because the spectrum simulates a Maxwell-Boltzmann distribution for a thermal energy of $kT = 25$ keV, the stellar average neutron capture cross sections could be derived from the experimental results with only minor corrections for deviations from the ideal spectrum. The measured cross sections were extrapolated to lower and higher thermal energies to cover the full temperature range of the *s*-process episodes in massive stars. The extrapolations for ^{74}Ge and ^{76}Ge were based on theoretical energy dependencies obtained by statistical model calculations, whereas for ^{75}As this information was adopted from evaluated nuclear data files.

The improved stellar cross sections have a significant impact on the abundance distribution of the weak *s*-process component associated with core He and shell C burning in massive stars. In particular, the *s*-process production of Ge in massive stars increases by up to 5% compared to calculations based on the previous MACSs. The abundance distribution of the weak *s* process exhibits a clear propagation effect starting at ^{74}Ge, by which the *s*-process efficiency is reduced by about 15%. However, this does not affect the *s* abundances of ^{76}Ge and ^{75}As, because the propagation effect is balanced by the new lower MACS values of both isotopes.

The considerably improved accuracy of the result for ^{76}Ge contributes to more reliable background estimates in double β decay experiments.

ACKNOWLEDGMENTS

We are grateful to the Van de Graaff crew M. Brock, E.-P. Knaetsch, and W. Seith for their strong support during the irradiations. R.G. acknowledges support by the Italian MIUR-PRIN06 Project "Late phases of Stellar Evolution: Nucleosynthesis in Supernovae, AGB stars, Planetary Nebulae." M.P. is supported by the Marie Curie Int. Reintegr. Grant MIRG-CT-2006-046520 within the European FP6, and by NSF grants PHY 02-16783 (JINA). R.R. is supported by the HGF Young Investigators Project VH-NG-327.

[1] R. Gallino *et al.*, Astrophys. J. **497**, 388 (1998).
[2] T. Rauscher, A. Heger, R. Hoffman, and S. Woosley, Astrophys. J. **576**, 323 (2002).
[3] C. Arlandini *et al.*, Astrophys. J. **525**, 886 (1999).
[4] S. Bisterzo, F. Käppeler, R. Gallino, M. Heil, and C. Domingo Pardo, in *Nuclei in the Cosmos IX*, edited by A. Mengoni *et al.* (SISSA, Trieste, 2006), contr. 077; http://pos.sissa.it/.
[5] C. Raiteri *et al.*, Astrophys. J. **419**, 207 (1993).
[6] C. Raiteri, M. Busso, R. Gallino, and G. Picchio, Astrophys. J. **371**, 665 (1991).
[7] M. Limongi, O. Straniero, and A. Chieffi, Astrophys. J. Suppl. **129**, 625 (2000).
[8] L. The, M. El Eid, and B. Meyer, Astrophys. J. **655**, 1058 (2007).
[9] M. Heil, F. Käppeler, E. Uberseder, R. Gallino, and M. Pignatari, Phys. Rev. C **77**, 015808 (2008).
[10] C. Kraus *et al.*, Eur. Phys. J. C **40**, 447 (2005).
[11] V. Lobashev, Nucl. Phys. **A719**, c153 (2003).
[12] F. Avignone, S. Elliott, and J. Engel, Rev. Mod. Phys. **80**, 481 (2008).
[13] H. Ejiri, Mod. Phys. Lett. A **22**, 1277 (2007).
[14] S. Elliott and J. Engel, J. Phys. G **30**, R183 (2004).
[15] G. Walter *et al.*, Astron. Astrophys. **167**, 186 (1986).
[16] Z. Bao *et al.*, At. Data Nucl. Data Tables **76**, 70 (2000).
[17] R. Anand, M. Jhingan, D. Bhattacharya, and E. Kondaiah, Nuovo Cimento A **50**, 247 (1979).
[18] R. Macklin, Nucl. Sci. Eng. **99**, 133 (1988).
[19] R. Macklin, N. Lazar, and W. Lyon, Phys. Rev. **107**, 504 (1957).
[20] H. Beer and F. Käppeler, Phys. Rev. C **21**, 534 (1980).
[21] W. Ratynski and F. Käppeler, Phys. Rev. C **37**, 595 (1988).
[22] J. de Laeter *et al.*, Pure Appl. Chem. **75**, 683 (2003).
[23] A. Farhan and B. Singh, Nucl. Data Sheets **86**, 785 (1999).
[24] A. Farhan and B. Singh, Nucl. Data Sheets **81**, 417 (1997).
[25] B. Singh, Nucl. Data Sheets **74**, 63 (1995).
[26] S. Agostinelli *et al.*, Nucl. Instrum. Methods A **506**, 250 (2003).
[27] S. Dababneh *et al.*, Nucl. Instrum. Methods A **517**, 230 (2004).
[28] J. Hubbell and S. Seltzer (2004), technical report, National Institute of Standards and Technology, Gaithersburg, MD; http://physics.nist.gov/PhysRefData/XrayMassCoef/.
[29] S. Mughabghab, in *Atlas of Neutron Resonances, 5th Edition* (Elsevier, Amsterdam, 2006).
[30] B. Allen, J. Gibbons, and R. Macklin, Adv. Nucl. Phys. **4**, 205 (1971).
[31] A. Lakshmana Rao and J. Rama Rao, Phys. Rev. C **6**, 572 (1972).
[32] A. Chaubey and M. Sehgal, Phys. Rev. **152**, 1055 (1966).
[33] S. Woosley, W. Fowler, J. Holmes, and B. Zimmerman, At. Data Nucl. Data Tables **22**, 371 (1978).
[34] M. Harris, Astrophys. Space Sci. **77**, 357 (1981).
[35] T. Rauscher and F.-K. Thielemann, At. Data Nucl. Data Tables **75**, 1 (2000).
[36] S. Goriely (2005), technical report, http://www-astro.ulb.ac.be/databases.html.
[37] C. Raiteri *et al.*, Astrophys. J. **367**, 228 (1991).
[38] M. Pignatari *et al.*, in *Nuclei in the Cosmos IX*, edited by A. Mengoni *et al.* (SISSA, Trieste, 2006), contr. 061; http://pos.sissa.it/.
[39] H. Klapdor-Kleingrothaus, I. Krivosheina, A. Dietz, and O. Chkvorets, Phys. Lett. **B586**, 198 (2004).
[40] H. Klapdor-Kleingrothaus, A. Dietz, I. Krivosheina, and O. Chkvorets, Nucl. Instrum. Methods A **522**, 371 (2004).
[41] A. Strumia and F. Vissani, hep-ph/0606054v2.

[42] Yu. Zdesenko, F. Danevich, and V. Trtyak, Phys. Lett. **B546**, 206 (2002).
[43] I. Abt *et al.* (GERDA Collaboration) (2005), GERDA Proposal to the LNGS P38/04; http://www.mpi-hd.mpg.de/gerda/.
[44] ENDF-LIBRARY, technical report, National Nuclear Data Center, Brookhaven National Laboratory (unpublished); www.nndc.bnl.gov/nndc/endf/.
[45] G. Meierhofer *et al.*, *Capture Gamma Ray Spectroscopy and Related Topics: 13th International Symposium*, edited by A. Blazhev, J. Jolie, N. Warr, and A. Zilges (AIP, New York, 2009), p. 559; Eur. Phys. J. A **40**, 61 (2009).
[46] B. Singh and D. Viggars, Nucl. Data Sheets **42**, 233 (1984).
[47] Z. Chunmei, Nucl. Data Sheets **95**, 59 (2002).